Ultrafast Electron Injection from Photoexcited Perovskite CsPbI$_3$ QDs into TiO$_2$ Nanoparticles with Injection Efficiency Near 99%

Feng Liu,[1] *Yaohong Zhang,*[1] *Chao Ding,*[1] *Taro Toyoda,*[1,6] *Yuhei Ogomi,*[2] *Teresa S. Ripolles,*[2] *Shuzi Hayase,*[2,6] *Takashi Minemoto,*[3,6] *Kenji Yoshino,*[4,6] *Songyuan Dai,*[5] *Qing Shen*,*[1,6]

[1]Faculty of Informatics and Engineering, The University of Electro-Communications,

1-5-1 Chofugaoka, Chofu, Tokyo 182-8585, Japan

[2]Faculty of Life Science and Systems Engineering, Kyushu Institute of Technology, 2-4

Hibikino, Wakamatsu-ku, Kitakyushu, Fukuoka 808-0196, Japan

[3]Department of Electrical and Electronic Engineering, Faculty of Science and

Engineering, Ritsumeikan University, 1-1-1 Nojihigashi, Kusatsu, Shiga 525-8577, Japan

[4]Department of Electrical and Electronic Engineering, Miyazaki University, 1-1 Gakuen,

Kibanadai Nishi, Miyazaki 889-2192, Japan

[5]Beijing Key Laboratory of Novel Thin Film Solar Cells, State Key Laboratory of

Alternate Electrical Power System with Renewable Energy Sources, North China Electric

Power University, Beijing 102206, P. R. China

[6]CREST, Japan Science and Technology Agency (JST), 4-1-8 Honcho, Kawaguchi,

Saitama 332-0012, Japan

AUTHOR INFORMATION

Corresponding Author:

*Qing Shen. E-mail: shen@pc.uec.ac.jp; Fax: +81424435501; Tel: +81424435471.

ABSTRACT

Photoexcited electron injection dynamics from $CsPbI_3$ quantum dots (QDs) to wide gap metal oxide nanoparticles are studied by transient absorption measurement. Experimental results show under the low pump pulse excitation ~99% of the photoexcited electrons in $CsPbI_3$ QDs can be injected into TiO_2 nanoparticles with a size-dependent rate constant ranged from 1.30×10^{10} to 2.10×10^{10} s^{-1}, which is also about 2.5 times faster than that in the case of ZnO. To investigate the implications of these findings in photovoltaic cells, a demonstration $CsPbI_3$ QD-sensitized solar cell based on $CsPbI_3$ QD-TiO_2 junctions is fabricated, which delivers a promising power conversion efficiency of 5%.

TOC Graphic
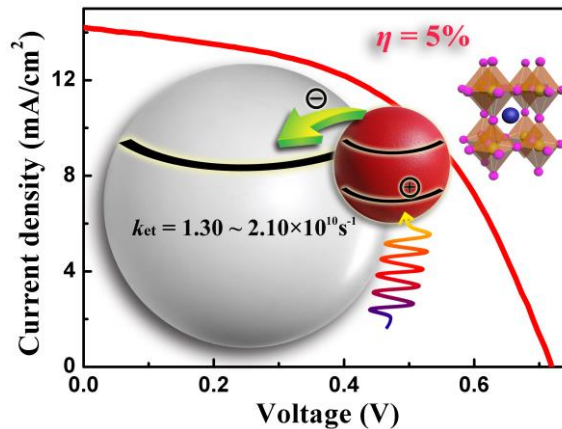
KEYWORDS: cesium lead iodide perovskite quantum dot, transient absorption spectroscopy, Marcus theory, quantum dot-sensitized solar cell, electron transfer dynamics

Semiconductor nanocrystals with the three-dimensional size below or equal to their exciton Bohr radius are the so called "quantum dots" (QDs). Over the past couple of years, much effort has been made to synthesize QD materials for use in solar cells due to their unique properties including size-tunable band gap, large extinction coefficients, and extended photostability.[1-8] Prominently, thermalization of photogenerated electrons in the QDs can be slowed by the phonon bottleneck.[9] What's more, potentially, QDs enable multiexciton generation, where multiple excited electron-hole pairs are generated following absorption of a single photon.[10] The above advantages of QDs hence allow to overcome the Schockley-Queisser limit for the power conversion efficiency of solar cells (31%).[9, 11-13]

Compared with the traditional classical QDs such as PbS and CdSe, lead halide perovskite QDs are newcomer nanomaterials that have been the subject of numerous recent studies.[14-19] Initially this family of perovskites is mostly studied as bulk thin films and inexpensive solar cells with conversion efficiencies exceeding 22% have been achieved using hybrid organic-inorganic perovskites.[20-29] Restricting the physical dimension of these perovskite crystallites to a few nanometers brings new attractive features such as large spectral tunability and extremely high luminescence (> 90% quantum yield without any further surface treatments).[30-33] Now, all-inorganic QDs of perovskite-type $CsPbX_3$ (X = Cl, Br, I) can be synthesized with precise size- and compositional control, offering highly bright and narrow band luminescence over the

whole visible wavelength range.[30, 32, 34-36] Following the success of colloidal synthesis, a variety of optoelectronic devices such as light-emitting devices, lasers, and photovoltaics have been demonstrated using $CsPbX_3$ QDs.[14, 37-42] Among the various $CsPbX_3$ perovskites with different compositions, $CsPbI_3$ stands out as one of the most attractive materials for use in solar cells because the light absorption of $CsPbI_3$ can exceed 700 nm by virtue of its narrower band gap (~1.73 eV in the bulk), while $CsPbBr_3$ and $CsPbCl_3$ have band gaps of ~2.25 eV and 3.05 eV, respectively.[43-44] In fact, a very impressive power conversion efficiency of up to 10% was achieved in thin film solar cells using $CsPbI_3$ QDs, which has surpassed most other QD solar cells.[37] In order to fully exploit the advantages of these perovskite QDs in solar cells, like the traditional implemented QDs, it is typically designed that QDs are selectively contacted with other materials of interest, for example with metal oxides (MOs) such as TiO_2, ZnO and SnO_2, to form a QD-MO junction.[45] The QD-MO junction constitutes an integral part of the solar cell, where the main charge separation process within the devices takes place. It thus imposes a great impact on the efficiency of the operating cells.[45-48] Understanding the electronic interactions between QDs and MOs is therefore essential in view of the fundamental physics and their potential application in optoelectronics. However, unlike the well-established traditional QD-MO systems such as PbS/TiO_2 and $CdSe/TiO_2$,[45, 49-52] to date, very little knowledge exists concerning the charge-transfer dynamics of the $CsPbI_3$ QD/MO nano-conjunctions, *i.e.*, the time scale of the electron transfer from $CsPbI_3$ QDs

5

to MOs has not been clearly determined. Transient absorption (TA) spectroscopy is a powerful tool capable of investigating ultrafast charge transfer across such interfaces of QD/MO.[45, 51-55] In this report, using TA measurement we present a comprehensive study of electron transport from colloidal $CsPbI_3$ QDs to the MO nanoparticles. An efficient electron injection from $CsPbI_3$ QDs to TiO_2 nanoparticles with a high injection efficiency of near 99% under low pump pulse excitation and a size-dependent injection rate constant are observed. Further, our studies show that $CsPbI_3$ QDs coupled with TiO_2 exhibit a more rapid electron transfer rate than that with ZnO. Initial $CsPbI_3$ QD-sensitized solar cells based on $CsPbI_3$ QD-TiO_2 junctions deliver a promising power conversion efficiency of 5%.
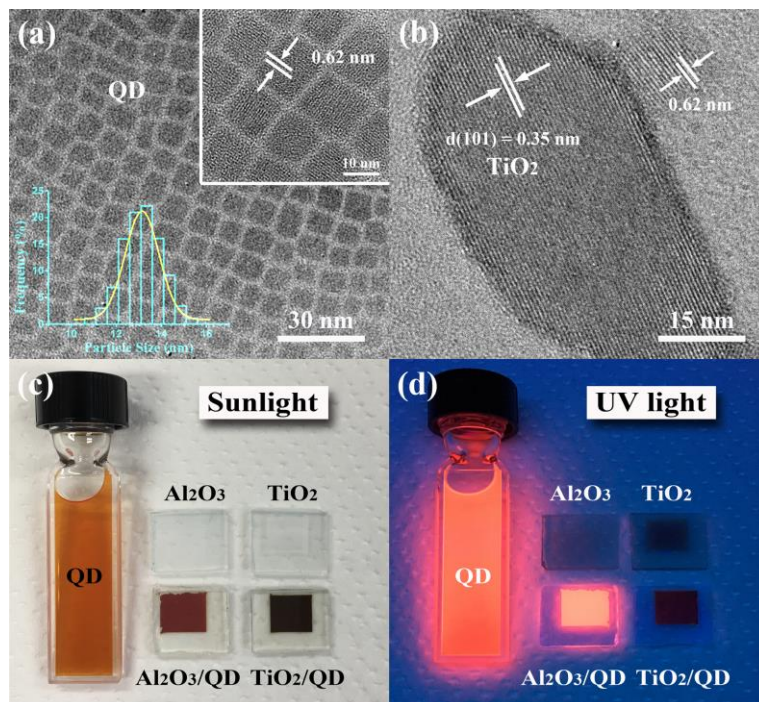

Figure 1. (a) Transmission electron microscopy (TEM) images of monodisperse $CsPbI_3$ QDs. The inset on the bottom left shows statistic analysis of size distribution for the

sample. (b) HRTEM image of the TiO_2-QD composite. (c) Pictures of QD solution, neat and QD-attached Al_2O_3 and TiO_2 films taken under sunlight and (d) under ultraviolet light.

Colloidal $CsPbI_3$ QDs with particle sizes ranging from ~10 to 15 nm were synthesized by literature procedure.[36] Purification of the as-synthesized QDs was carried out as described by Swarnkar *et al*. and the resulting QDs dispersed in hexane can be phase-stable for months.[37] Figure 1a shows typical TEM images of the $CsPbI_3$ QDs as well as their size distribution. The lattice fringe with a spacing of 0.62 nm can be assigned to (100) plane of the cubic phase $CsPbI_3$. The adsorption of the QDs on TiO_2 or Al_2O_3 was performed by directly immersing the TiO_2 or Al_2O_3 films into $CsPbI_3$ QD hexane solution. The adsorption process was kept in dark for 24 h. Afterwards, the films were washed thoroughly with hexane and dried in N_2 atmosphere. Figure 1b shows a typical high-resolution TEM image of $CsPbI_3$ QDs with a size of ~12 nm attached to a TiO_2 nanoparticle after adsorption. The measured interplanar spacings of 0.35 nm and 0.62 nm respectively confirm the presence of $CsPbI_3$ QDs on TiO_2 surface. Notably, it was observed that there is an epitaxial interface between the TiO_2 and the QDs, indicating a direct contact and hence the loss of QD surface ligands at the interface of QD/TiO_2. Such ligand detachment from surface of the QDs is also implied in Guijarro *et al*.'s report, where part of the surface ligand on CdSe QDs was removed when QDs are directly contacted with TiO_2.[56] A possible reason for this is that intermolecular interactions

7

between QDs and TiO$_2$ could be stronger than that with its initial surface ligands (*i.e.*, oleylammonium oleate). The inset in Figure 1c shows photos of the TiO$_2$ and Al$_2$O$_3$ films before and after incorporation of the CsPbI$_3$ QDs. The deep color observation of the film samples after adsorption suggests a considerable amount of QDs on both films.

The prepared colloidal CsPbI$_3$ QDs with different particle sizes exhibit size-dependent emissions from 640 to 680 nm, characterized by narrow emission line widths of 30~40 nm and high quantum yields reaching 90%, indicating that they are highly luminescent in the visible range. As expected, as shown in Figure 1d, bright fluorescence emission from QDs dispersed in colloidal solution or deposited on Al$_2$O$_3$ films can be seen under ultraviolet radiation. However, compared to QDs on Al$_2$O$_3$ films, photoluminescence of the CsPbI$_3$ QDs was significantly quenched upon contacting with TiO$_2$. This effect indicates that electron transfer occurs on TiO$_2$ surface but not on Al$_2$O$_3$. Further, the disappearance of the PL emission signal in QD/TiO$_2$ sample shown in Figure S1 also supports this observation and confirms the effective electron transfer from photoexcited QDs to TiO$_2$.
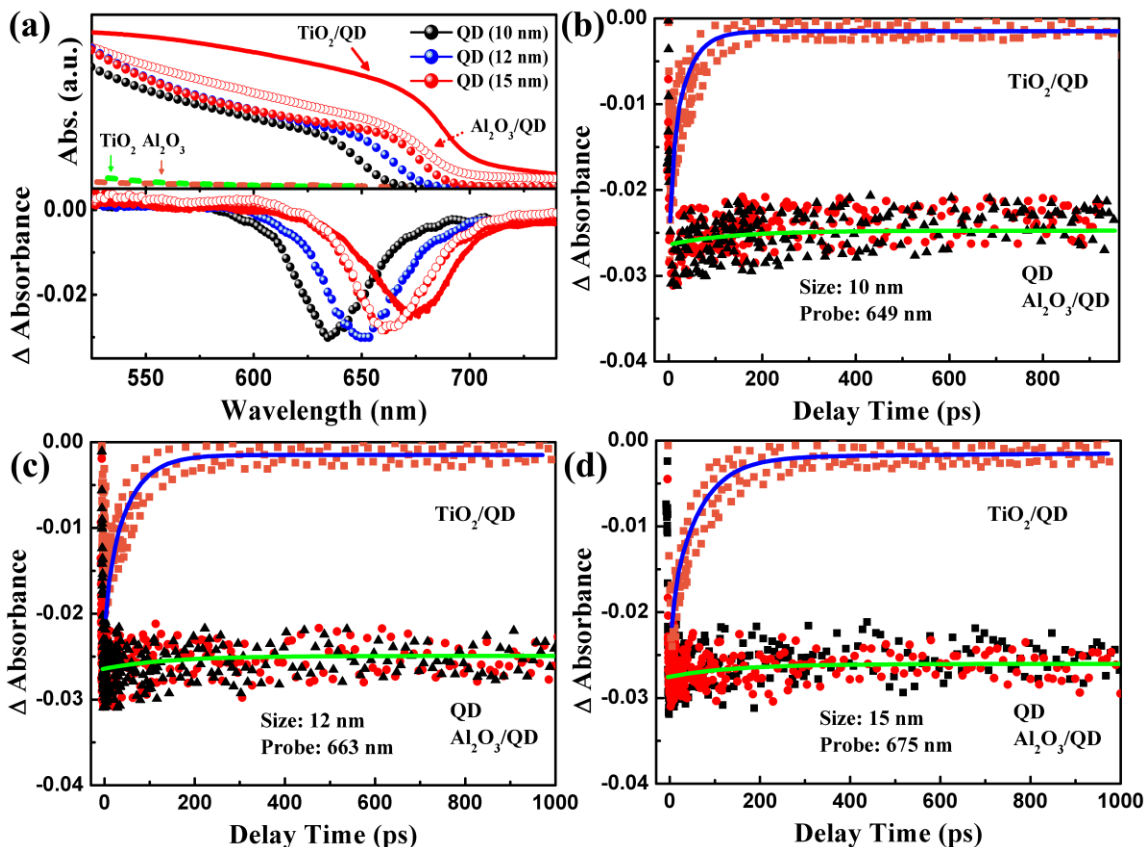
Figure 2. (a) Steady-state UV-visible (top half) and transient absorption spectra (bottom half) of the CsPbI$_3$ QDs with different particle sizes dispersed in hexane and adsorbed on TiO$_2$ and Al$_2$O$_3$ mesoporous films (15 nm-QD). TA spectra were recorded 5 ps after bandgap excitation with excitation wavelength of 470 nm and power intensity of 0.5 μJ/cm^2. (b-d) TA kinetic traces of different-sized CsPbI$_3$ QDs dispersed in hexane and attached to TiO$_2$ and Al$_2$O$_3$ substrates. Excitation wavelength is 470 nm and power intensity is 0.5 μJ/cm^2. Solid line shows exponential fit to the TA dynamics.

To obtain direct evidence of electron transfer from CsPbI$_3$ QDs to TiO$_2$ and, furthermore, to evaluate the rate of this reaction, femtosecond TA spectroscopy was employed. The top half of Figure 2a shows steady-state UV-vis absorption spectra of

9

different size CsPbI$_3$ QDs and those (QD size: ~15 nm) attached to TiO$_2$ and Al$_2$O$_3$ films. It is clearly shown that the excitonic peak of the CsPbI$_3$ QDs blue shifts with decreasing particle size as a result of quantum confinement effect.[57] Meanwhile, interestingly, CsPbI$_3$ QDs adsorbed on Al$_2$O$_3$ surface show similar excitonic absorption peak position as in the solution, while that of peak in the case of TiO$_2$ seems to be slightly red shifted, which is more pronouncedly reflected in its TA spectrum, as described below. The bottom half of Figure 2a shows the TA spectra of these various different samples recorded 5 ps after bandgap excitation. The bleaching maximum of each coincides with the exciton absorption seen in the steady-state absorption spectrum. Now, a notable exciton peak shift from 663 to 674 nm is observed when QDs are adsorbed on TiO$_2$. Such red shift can originate from the difference in dielectric environment of the surface bound CsPbI$_3$ QDs when compared to the solution, which leads to a change in the total energy of an exciton confined to the QDs (dielectric constants of CsPbI$_3$, hexane, Al$_2$O$_3$, and TiO$_2$ are 6.0, 2.0, 4.5, and 80, respectively), as described previously.[58-60]

Before proceeding to a detailed analysis of the electron transfer dynamics using TA measurement, three-body Auger recombination process in CsPbI$_3$ QDs is studied and eliminated as the Auger time scale in QDs could potentially overlap with that of the charge transfer between nanoparticles and tend to complicate the discussion.[15, 61-65] Figure S2 shows the dependence of the normalized TA decays on pump excitation intensities for the different-sized QDs dispersed in hexane. For the studied three kinds of QDs, fast

decay processes appear in their TA responses when the pump intensity is larger than 0.5 μJ/cm^2, and the TA responses decay faster as the pump intensity increases further. This observation indicates the presence of three-body Auger recombination process in CsPbI$_3$ QDs under the high pump intensity excitation.[61, 65-67] However, when the pump intensity is smaller than 0.5 μJ/cm^2, we found the fast decay process disappeared and the waveforms of the TA responses overlapped with each other very well when they were normalized at the peak intensity within 1 ns. This means that the three-body Auger recombination process is negligible under such low pump intensity excitation. Therefore, in the following, for the TA measurements, samples will be excited with pump intensity of 0.5 μJ/cm^2 to eliminate the potential effects of Auger process. Figure 2b, 2c, 2d show the TA trace of the three different size CsPbI$_3$ QDs unattached (*i.e.*, in solution) and attached (*i.e.*, adsorbed) to TiO$_2$ and Al$_2$O$_3$ films recorded at their bleaching maximum. It is found that the TA kinetics of these unattached QDs can be well fitted using the following single-exponential function with a constant component y_0:

$$Y(t) = A_0 \exp(\frac{-t}{\tau}) + y_0 \quad (1)$$

Fitting the TA kinetics of each sample to the above eq (1) gives a decay time constant τ_{QD} of 387 ps, 420 ps, and 430 ps ($A_0/(A_0+y_0) = 0.1$) for 10 nm-, 12 nm-, and 15 nm-QDs, respectively. It is noted that the measured TA dynamics for the unattached CsPbI$_3$ QDs are in good line with previous reports.[65, 68] Given the absence of three-body Auger recombination process at the present measuring conditions, the fitted time constant τ_{QD}

can be assigned to one-body non-radiative recombination in the QDs, *i.e.*, electron and/or hole trapping in defect states (more experimental evidence to this assignment can be found in Supporting Information, Figure S3).[30, 61, 67] The constant component y_0 is assigned to two-body radiative recombination in the QDs (*i.e.*, photoluminescence process), which has lifetime >> 1 ns. The component proportion of $y_0/(A_0+y_0) = 0.9$ thus explains the previous measured photoluminescence quantum yield of ~90% for the CsPbI$_3$ QDs. Further, significantly, it is found the TA signal decay of the QDs attached on TiO$_2$ becomes much faster than that of the unattached QDs (dispersed in hexane), while TA trace on Al$_2$O$_3$ shows no apparent change on the time scale of the measurement. The above difference is indicative of electron transfer from the conduction band of the CsPbI$_3$ QDs to TiO$_2$ but not to Al$_2$O$_3$. This can be understood by the energy level diagrams of the Al$_2$O$_3$, TiO$_2$, and CsPbI$_3$ QDs as shown in Figure 4a, from which we can see the conduction band minimum of Al$_2$O$_3$ is much higher than that of the QDs. TA decays of the QDs on TiO$_2$ films show single exponential kinetics with time constant $\tau_{QD+TiO2}$ of 42 ps, 50 ps, and 65 ps ($A_0/(A_0+y_0) = 0.9$) for 10 nm-, 12 nm-, and 15 nm-QDs, respectively. Kinetic parameters of the fits for all samples are summarized in Table S1. As indicated in previous reports,[54, 69-71] in the absence of a hole acceptor, TA bleach near band gap of the QDs attached to TiO$_2$ is associated with both electron and hole in the photoexcited QDs, *i.e.*, trapping of electron and/or hole, Auger recombination, electron relaxation to the ground state, and backward charge recombination between injected electron and the hole.

Considering the absence of Auger recombination process as stated above and the much longer lifetime of the backward charge recombination process when compared with that of the electron injection process typically found in previous reports,[54] the TA bleach near band gap of the QDs should be dominated by electron transfer process from QDs to TiO$_2$. The electron injection is also confirmed by the considerable photocurrent obtained for the CsPbI$_3$ QD-sensitized TiO$_2$ solar cells, which will be discussed in the following. The background signal y_0 here with lifetime >1 ns can be assigned to electron relaxation to the ground state and backward charge recombination between injected electrons and the holes. Further, if we assume the electron transfer is the only added pathway for the excited-state interaction between QDs and TiO$_2$, then the electron transfer rate $k_{(QD/TiO2)}$ from QDs to TiO$_2$ can be given by $k_{(QD/TiO_2)} = 1/\tau_{(QD+TiO_2)} - 1/\tau_{(QD)}$, based on which we calculated an effective electron transfer rate $k_{(QD/TiO2)}$ of 2.10×10^{10} s^{-1}, 1.76×10^{10} s^{-1}, and 1.30×10^{10} s^{-1} for 10 nm-, 12 nm-, and 15 nm-QDs, respectively. The electron injection efficiency η_{inj} from CsPbI$_3$ QDs to TiO$_2$ can be given by the following equation:

$$\eta_{inj} = C_{QD} \frac{k_{(QD/TiO_2)}}{k_{(QD/TiO_2)} + k_{QD}} + C_{PL} \frac{k_{(QD/TiO_2)}}{k_{(QD/TiO_2)} + k_{PL}} \quad (2)$$

where C_{QD} and C_{PL} are component proportions of one-body charge carrier trapping process and two-body radiative recombination process (*i.e.*, photoluminescence) in the free QDs, respectively, k_{QD} and k_{PL} are their corresponding rate constants, $k_{QD} = 1/\tau_{QD}$, $k_{PL} = 1/\tau_{PL}$, and $k_{(QD/TiO2)}$ is electron transfer rate from QDs to TiO$_2$. Taking 12 nm-QD as an example, the C_{QD} and C_{PL} values have been determined to be ~0.1 (*i.e.*, $A_0/(A_0+y_0)$ in

13

free QDs) and 0.9 (*i.e.*, $y_0/(A_0+y_0)$ in free QDs), respectively, $k_{(QD/TiO2)}$ is 1.76×10^{10} s^{-1}, k_{QD} is 0.24×10^{10} s^{-1}, and $k_{PL} \ll 0.1 \times 10^{10}$ s^{-1} (because photoluminescence lifetime τ_{PL} $\gg 1$ ns). Therefore, eq (2) leads to η_{inj} value reaching almost 99%, which means that about 99% of the photoexcited electrons in the CsPbI$_3$ QDs can be injected into TiO$_2$ nanoparticles.
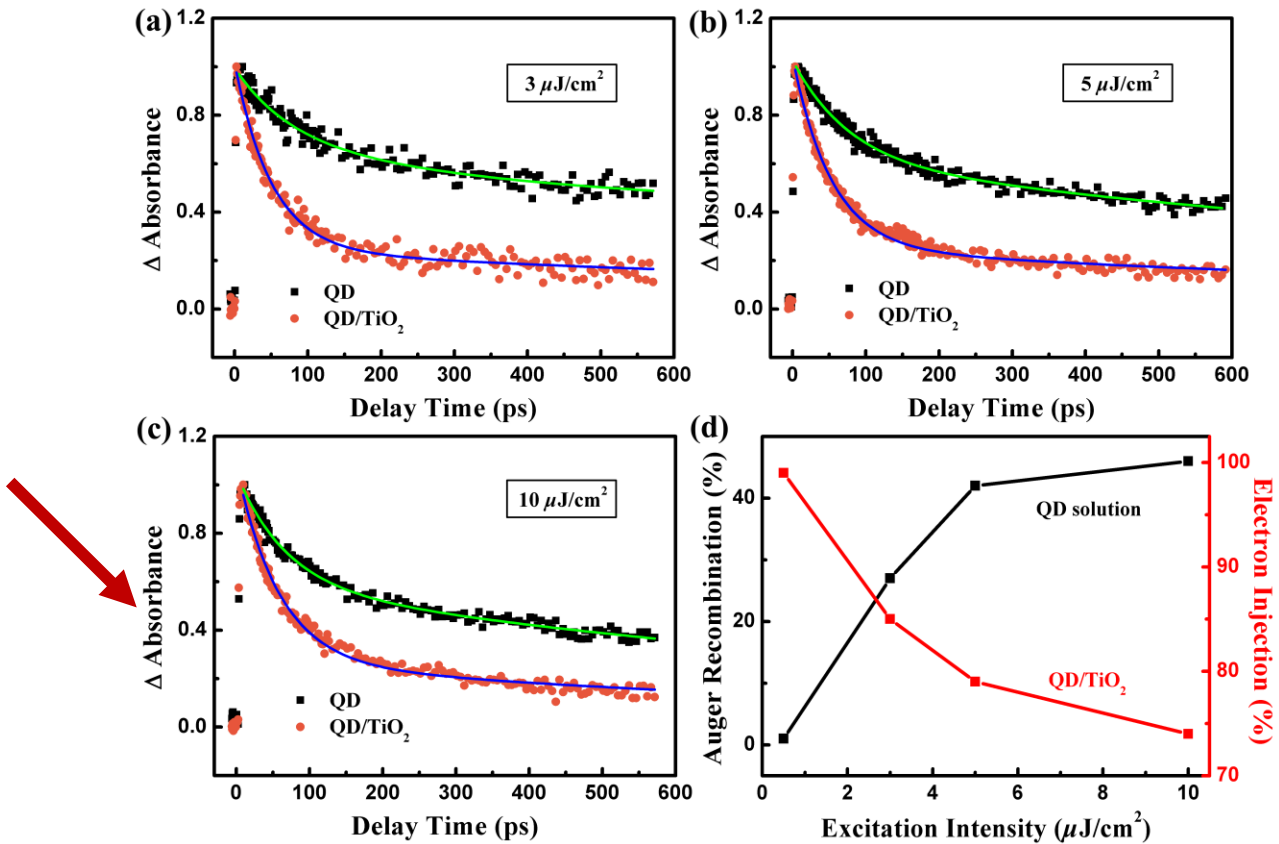

Figure 3. (a-c) Normalized TA responses for the free standing QDs and QD/TiO$_2$ composite measured under different excitation intensity. (d) Dependence of the fractional amplitude of Auger recombination in QDs and electron injection efficiency on excitation power.

Previous studies probing electron injection from dye to TiO_2 can observe a clear absorption signal around 1000 nm in TA spectra, which corresponds to those electrons that have been injected into TiO_2.[72-74] Therefore, additionally, for $CsPbI_3$ QD/TiO_2 system, we also carried out TA measurement, expecting to observe similar absorption signal to prove directly the injection of the photoexcited electrons. To do so, probe wavelength in TA spectra was changed to near infrared region of 800 to 1600 nm and a low excitation intensity of 0.5 $\mu J/cm^2$ was first used (pump wavelength was kept as 470 nm), under which condition Auger process is negligible and the electron injection efficiency can reach 99% as revealed before through probe of the QDs. However, from TA spectra, throughout the whole probe range we can not observe clear absorption signal that can be considered processible. This can be due to the low pump intensity used, *i.e.*, although the electron injection efficiency can reach 99%, the total amount of the photoexcited electrons is limited under such low pump intensity. Therefore, we assume unlike the "indirect" way probing on the photoexcited QDs (the probe wavelength of 649-679 nm) which features high response even at the low excitation intensity, direct probe on the injected electrons in TiO_2 requires a higher excitation intensity so as to guarantee a high concentration of the electrons in TiO_2 and therefore meet the minimum requirement for TA response.[72] So, next, the excitation intensity was increased from 0.5 to 10 $\mu J/cm^2$ (further increasing the intensity causes damage of the QDs as white spot appears after pump pulse excitation). However, it turns out that TA spectra still do not have the necessary signal to noise ratio

that can be processed as an indicator of the injected electrons. The reason behind this is investigated in detail and we found an unusual Auger recombination behavior in $CsPbI_3$ QDs, which is actually not the case in most dye sensitizers. In the following we will show that the $CsPbI_3$ QDs suffer from a severe Auger recombination process, which reduces greatly the total amount of the photoexcited electrons that can be injected into TiO_2 for larger excitation intensity. Figure 3a-c present TA kinetic traces of the free standing QDs (*i.e.*, QD solution) and the QD/TiO_2 composite under different excitation intensities. Kinetic parameters of the fits are summarized in Table S2 (Supporting Information), from which we see a significant Auger recombination in $CsPbI_3$ QDs even at moderate excitation intensity and has a long life-time of ~75 ps, comparable to that of the electron injection process of ~50 ps. Fractional amplitude of the Auger recombination in free QDs and the corresponding electron injection efficiency from QDs to TiO_2 under different excitation intensities are plotted in Figure 3d (electron injection efficiency was calculated using eq 2 by replacing charge carrier trapping parameters with that of Auger process). It clearly shows that degree of the Auger recombination process accelerates with the increase of excitation intensity, leading to ~30% loss of the total photoexcited electrons that should have been injected into TiO_2 under moderate excitation intensity of 10 $\mu J/cm^2$. The prominent Auger recombination process demonstrated here is in line with Liu *et al*.'s report, where they found Auger recombination exists in the relaxation process of $CsPbI_3$ QDs even though the number of exciton in nanocrystals is as low as 0.67.[65] In order to

increase the concentration of the injected electrons in TiO_2, we should further increase the excitation intensity, however, as mentioned before, this would cause damage of the QDs. Due to the reasons above, unfortunately, we can not directly probe the injected electrons in TiO_2 under the present conditions. But we notice another attempt to directly observe the injected electrons from QDs to TiO_2 or ZnO, where Stockwell *et al.* employed IR transient absorption measurement with a probe wavelength of 5000 nm to investigate the injection process from CdSe QDs to TiO_2.[69] Note that CdSe QDs also suffer from a certain degree of Auger recombination loss. Since the absorption coefficient of free carriers in a semiconductor (*i.e.*, the electrons injected to the TiO_2 electrode here) at longer IR wavelength such as 5000 nm is much larger than that at shorter wavelengths such as 800-1600 nm used in our TA setup, it would be better to detect the injected electrons in TiO_2 directly using the longer IR probe wavelength in the TA measurements. However, due to our limited lab equipment availability, we are not able to conduct such experiment right now, further work is still needed.
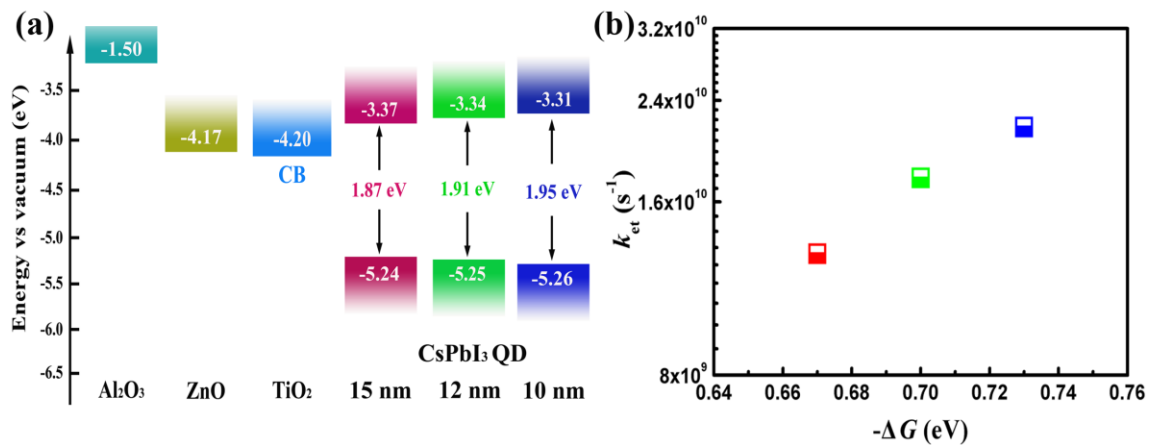
Figure 4. (a) Schematic energy level diagrams of the MOs and CsPbI$_3$ QDs with various

particle sizes. (b) Electron transfer rate constant as a function of the free energy change ΔG.

Electron transfer kinetics in a quantized semiconducting nanocrystal donor and nanoparticulate metal oxide acceptor system has been evaluated in terms of Marcus theory.[45, 49-50, 75-76] The functional form of Marcus model is described as follows:

$$k_{et} = \frac{2\pi}{h} \int_{-\infty}^{\infty} \rho(E) \left| \overline{H}(E) \right|^2 \frac{1}{\sqrt{4\pi\lambda k_B T}} e^{-\frac{(\lambda+\Delta G+E)^2}{4\lambda k_B T}} dE \quad (3)$$

where k_{et} is the charge transfer rate, $\hbar$ is the reduced Planck's constant, $\rho(E)$ is density of states of acceptor, $\overline{H}(E)$ stands for overlap matrix element, k_B is Boltzmann's constant, T is temperature, λ is the system reorganizational energy, ΔG is the free energy change between the donor and acceptor systems. Under assumption that overlap matrix element $\overline{H}(E)$ does not significantly depend on energy, we can see the logarithm of the electron transfer rate is a quadratic function of the free energy change, $i.e.$, ΔG. In our specific QD-TiO$_2$ system, there are three major factors which contribute to ΔG: free energy of charging, free energy of coulombic interactions, and the change in electronic energy. Therefore, ΔG can be given by the following expression:[45]

$$\Delta G = E_{TiO_2} - E_{QD} + \frac{e^2}{2R_{QD}} + \frac{2.2e^2}{\varepsilon_{QD}R_{QD}} - \frac{e^2}{4(R_{QD}+l)} \frac{\varepsilon_{TiO_2}-1}{\varepsilon_{TiO_2}+1} \quad (4)$$

where E_{TiO2} and E_{QD} are conduction band minimum energies of TiO$_2$ and QD, respectively, e is the elementary charge, R_{QD} and ε_{QD} are radius and dielectric constant of the QDs, ε_{TiO2} is dielectric constant of TiO$_2$, l is QD-TiO$_2$ separation distance. A depiction of energy state

alignment for the $CsPbI_3$ and TiO_2 under investigation is shown in Figure 4a. Note that

the exact band gap for each size QD is determined from their TA spectra using TA bleach

peak measured under the low excitation intensity (Figure S2). Valence band energy is

derived from photoelectron yield spectroscopy (PYS) measurement, see Figure S4.

According to the above measured band energies and the previously reported values for

$CsPbI_3$ and TiO_2 (*e.g.*, ε_{QD} = 6.003, ε_{TiO2} = 80),[77-78] we calculated the ΔG values for

$CsPbI_3$ QD-TiO_2 system ranging from ~0.67 to 0.73 eV, which are varied with QD size

(note that l is set to be 0 nm because the distance between QDs and TiO_2 is negligible

compared to QD size). In Figure 4b, the electron transfer rate from $CsPbI_3$ QDs to TiO_2

with respect to ΔG is plotted. It clearly reflects that the small energy difference attained by

changing particle size of the QDs has led to a considerable variation in the transfer

kinetics. In fact, plot of k_{et} vs. ΔG for various reorganizational energies has been studied

in Tvrdy *et al*.'s report,[45] from which we can learn that in the reorganizational energy

dominated region, where $\Delta G \leq \lambda$ (λ is system reorganizational energy), the electron

transfer dynamics is greatly dependent on the energy ΔG, while in the region where $\Delta G >$

λ, the transfer rate constant is dominated by the density of electron accepting states, *i.e.*,

$\rho(E)$, and less dependent on ΔG. For $CsPbI_3$ perovskite material in our case, the λ value

was previously estimated to be ~1642 meV,[79] which is much larger than our calculated ΔG

values of 670~730 meV. Therefore it is reasonable to see that the small difference in ΔG

in $CsPbI_3$ QD system induces such a noticeable change in transfer rate as recorded in
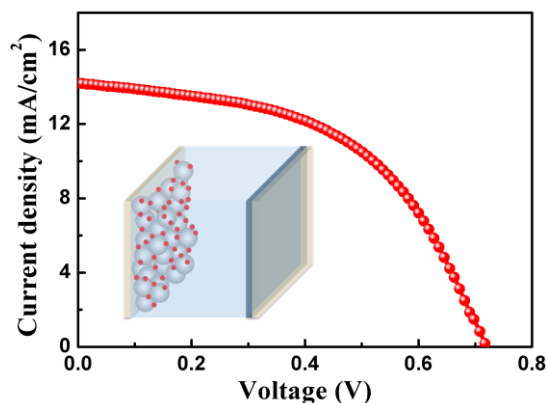
Figure 4b.
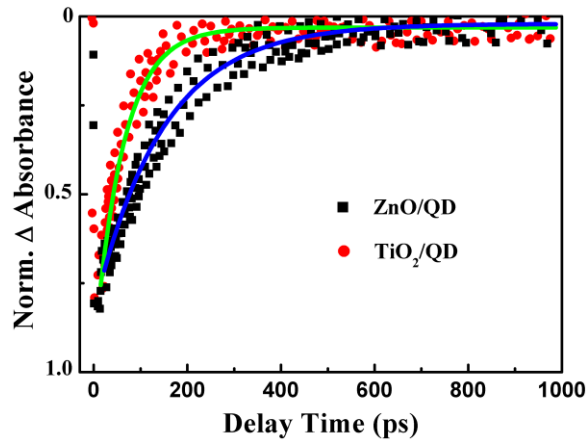
Figure 5. Comparison of the TA dynamics of 12 nm-CsPbI$_3$ QDs attached to TiO$_2$ and ZnO. The samples were excited at a wavelength of 470 nm with power intensity of 0.5 μJ/cm^2. Solid line shows exponential fit to the TA dynamics.

Also, we have carried out TA measurement on the samples of QD-ZnO composite. Figure 5 shows that compared to the TA trace of the QDs attached to TiO$_2$, QD-ZnO composite exhibits slower TA decay dynamics with charge transfer rate of 0.70×10^{10} s^{-1}, which is almost 2.5 times slower than that in the case of TiO$_2$ (1.76×10^{10} s^{-1}). ΔG values calculated for QD-ZnO system are ranged from 0.64 to 0.71 eV, also depending on QD size and about 0.03 eV smaller than that in QD-TiO$_2$ system. But of course, according to eq (3), the difference of charge transfer dynamics between two QD-MO systems can not only attribute to the difference in ΔG value but also related to the difference in both coupling degree between two nanoparticles (*i.e.*, $\overline{H}(E)$) and the density of accepting states in acceptors (*i.e.*, $\rho(E)$). In addition to Marcus theory, we note that for electron injection process from an adsorbate to ZnO, it is also possible that the electron transfer

20

rate is influenced by the presence of a certain intermediate state, as demonstrated in previous reports.[69, 80] For example, Stockwell *et al.* found a long-lived interface-bound charge-separated pair (IBCSP) state in Coumarin 343/ZnO system, which plays key role in determining the electron transfer rate across the interface.[69]

Figure 6. Current-voltage (*J-V*) characteristic of the CsPbI$_3$ QD-sensitized TiO$_2$ solar cells under 100 mW/cm^2 illumination. The inset shows device architecture for the fabricated solar cells.

The ability to inject photoexcited electrons to TiO$_2$ renders CsPbI$_3$ QDs extremely suitable for use in QD-sensitized solar cells (QDSCs). Therefore, we fabricated prototype QDSCs with CsPbI$_3$ QDs as the sensitizer. Mesoporous films of ~30 nm-TiO$_2$ nanoparticles with thickness of ~15 μm were prepared to deposit the 12 nm-CsPbI$_3$ QDs; Liquid-state iodide electrolyte (I$^-$/I$_3^-$) was used to scavenge the photoexcited holes in the QDs (details of the fabrication can be found in Supporting Information). Power conversion efficiency of the resulting solar cells reaches 5% with open-circuit voltage of 0.72 V, short-circuit current density of 14.17 mA/cm^2, and fill factor of 0.49 (Figure 6).

Considering that no attempt was made to construct the $CsPbI_3$ QD-sensitized solar cells and to optimize the performance (*e.g.*, liquid electrolyte and TiO_2 film thickness, *etc.*), the results are encouraging, and we notice that the efficiency obtained at this stage is slightly higher than that of the first solar cell demonstration of the nanocrystalline $CH_3NH_3PbI_3$, which employed the same cell configuration as well as the same I^-/I_3^- electrolyte as ours, and exhibited efficiency of 3.8%,[81] suggesting that $CsPbI_3$ may possess greater potential for use in high-efficiency solar cells.

We have presented experimental results which show direct evidence of electron injection from photoexcited $CsPbI_3$ QDs to the metal oxides (TiO_2 and ZnO) on a picosecond time scale. Apparent electron transfer rate constants from QDs to TiO_2 exhibited strong dependence on particle size of the QDs ranged from 1.30×10^{10} to 2.10×10^{10} s^{-1}, which can be rationalized by Marcus theory. In addition, we elucidate that the electron injection efficiency can reach almost 99% under the low pump pulse excitation. Further, electron transfer dynamics from $CsPbI_3$ QDs to TiO_2 was proven to be about 2.5 times faster than that to ZnO. As a demonstration of $CsPbI_3$ QD application in sensitized solar cells, liquid-state $CsPbI_3$ QD-sensitized solar cells were fabricated based on TiO_2 mesoporous films, which showed a promising power conversion efficiency of 5%.

ASSOCIATED CONTENT

Supporting Information. Experimental details, steady-state photoluminescence, TA

spectra, TA kinetic parameters, PYS spectra. This material is available free of charge *via* the Internet at http://pubs.acs.org.

AUTHOR INFORMATION

Corresponding Author

shen@pc.uec.ac.jp

Notes

The authors declare no competing financial interest.

ACKNOWLEDGMENT

REFERENCES

1. Pattantyus-Abraham, A. G.; Kramer, I. J.; Barkhouse, A. R.; Wang, X.; Konstantatos, G.; Debnath, R.; Levina, L.; Raabe, I.; Nazeeruddin, M. K.; Gratzel, M. Depleted-Heterojunction Colloidal Quantum Dot Solar Cells. *ACS Nano* **2010**, *4*, 3374-3380.

2. Kamat, P. V. Quantum Dot Solar Cells. Semiconductor Nanocrystals as Light Harvesters. *J. Phys. Chem. C* **2008**, *112*, 18737-18753.

3. Rühle, S.; Shalom, M.; Zaban, A. Quantum‐Dot‐Sensitized Solar Cells. *ChemPhysChem* **2010**, *11*, 2290-2304.

4. González-Pedro, V.; Xu, X.; Mora-Sero, I.; Bisquert, J. Modeling High-Efficiency Quantum Dot Sensitized Solar Cells. *ACS Nano* **2010**, *4*, 5783-5790.

5. Sargent, E. H. Colloidal Quantum Dot Solar Cells. *Nat. Photonics* **2012**, *6*, 133-135.

6. Pan, Z.; Mora-Seró, I. n.; Shen, Q.; Zhang, H.; Li, Y.; Zhao, K.; Wang, J.; Zhong, X.; Bisquert, J. High-Efficiency "Green" Quantum Dot Solar Cells. *J. Am. Chem. Soc.* **2014**, *136*, 9203-9210.

7. Zhang, J.; Gao, J.; Church, C. P.; Miller, E. M.; Luther, J. M.; Klimov, V. I.; Beard, M. C. PbSe Quantum Dot Solar Cells with More than 6% Efficiency Fabricated in Ambient Atmosphere. *Nano Lett.* **2014**, *14*, 6010-6015.

8. Du, Z.; Pan, Z.; Fabregat-Santiago, F.; Zhao, K.; Long, D.; Zhang, H.; Zhao, Y.; Zhong, X.; Yu, J.-S.;

Bisquert, J. Carbon Counter-Electrode-Based Quantum-Dot-Sensitized Solar Cells with Certified Efficiency Exceeding 11%. *J. Phys. Chem. Lett.* **2016**, *7*, 3103-3111.

9. Nozik, A. Quantum Dot Solar Cells. *Phys. E* **2002**, *14*, 115-120.

10. Sambur, J. B.; Novet, T.; Parkinson, B. Multiple Exciton Collection in a Sensitized Photovoltaic System. *Science* **2010**, *330*, 63-66.

11. Nozik, A. J. Multiple Exciton Generation in Semiconductor Quantum Dots. *Chem. Phys. Lett.* **2008**, *457*, 3-11.

12. McGuire, J. A.; Joo, J.; Pietryga, J. M.; Schaller, R. D.; Klimov, V. I. New Aspects of Carrier Multiplication in Semiconductor Nanocrystals. *Acc. Chem. Res.* **2008**, *41*, 1810-1819.

13. Watson, D. F. Linker-Assisted Assembly and Interfacial Electron-Transfer Reactivity of Quantum Dot-Substrate Architectures. *J. Phys. Chem. Lett.* **2010**, *1*, 2299-2309.

14. Song, J.; Li, J.; Li, X.; Xu, L.; Dong, Y.; Zeng, H. Quantum Dot Light-Emitting Diodes Based on Inorganic Perovskite Cesium Lead Halides (CsPbX3). *Adv. Mater.* **2015**, *27*, 7162-7167.

15. Rainò, G.; Nedelcu, G.; Protesescu, L.; Bodnarchuk, M. I.; Kovalenko, M. V.; Mahrt, R. F.; Stöferle, T. Single Cesium Lead Halide Perovskite Nanocrystals at Low Temperature: Fast Single-Photon Emission, Reduced Blinking, and Exciton Fine Structure. *ACS Nano* **2016**, *10*, 2485-2490.

16. Protesescu, L.; Yakunin, S.; Kumar, S.; Bär, J.; Bertolotti, F.; Masciocchi, N.; Guagliardi, A.; Grotevent, M.; Shorubalko, I.; Bodnarchuk, M. I. Dismantling the "Red Wall" of Colloidal Perovskites: Highly Luminescent Formamidinium and Formamidinium-Cesium Lead Iodide Nanocrystals. *ACS Nano* **2017**, *11*, 3119-3134.

17. Yettapu, G. R.; Talukdar, D.; Sarkar, S.; Swarnkar, A.; Nag, A.; Ghosh, P.; Mandal, P. Terahertz Conductivity within Colloidal CsPbBr3 Perovskite Nanocrystals: Remarkably High Carrier Mobilities and Large Diffusion Lengths. *Nano Lett.* **2016**, *16*, 4838-4848.

18. Liu, F.; Ding, C.; Zhang, Y.; Ripolles, T. S.; Kamisaka, T.; Toyoda, T.; Hayase, S.; Minemoto, T.; Yoshino, K.; Dai, S.; Yanagida, M.; Noguchi, H.; Shen, Q. Colloidal Synthesis of Air-Stable Alloyed CsSn1-xPbxI3 Perovskite Nanocrystals for Use in Solar Cells. *J. Am. Chem. Soc.* **2017**, *139*, 16708-16719.

19. Li, C.; Guerrero, A.; Zhong, Y.; Gräser, A.; Luna, C. A. M.; Köhler, J.; Bisquert, J.; Hildner, R.; Huettner, S. Real-Time Observation of Iodide Ion Migration in Methylammonium Lead Halide Perovskites. *Small* **2017**, *13*, 1701711.

20. Ball, J. M.; Lee, M. M.; Hey, A.; Snaith, H. J. Low-Temperature Processed Meso-Superstructured to Thin-Film Perovskite Solar Cells. *Energy Environ. Sci.* **2013**, *6*, 1739-1743.

21. Grätzel, M. The Light and Shade of Perovskite Solar Cells. *Nat. Mater.* **2014**, *13*, 838-842.

22. Im, J.-H.; Lee, C.-R.; Lee, J.-W.; Park, S.-W.; Park, N.-G. 6.5% Efficient Perovskite Quantum-Dot-Sensitized Solar Cell. *Nanoscale* **2011**, *3*, 4088-4093.

23. Jeon, N. J.; Lee, J.; Noh, J. H.; Nazeeruddin, M. K.; Grätzel, M.; Seok, S. I. Efficient Inorganic-Organic Hybrid Perovskite Solar Cells Based on Pyrene Arylamine Derivatives as Hole-Transporting Materials. *J. Am. Chem. Soc.* **2013**, *135*, 19087-19090.

24. McGehee, M. D. Perovskite Solar Cells: Continuing to Soar. *Nat. Mater.* **2014**, *13*, 845-846.

25. Snaith, H. J. Perovskites: The Emergence of a New Era for Low-Cost, High-Efficiency Solar Cells. *J. Phys. Chem. Lett.* **2013**, *4*, 3623-3630.

26. Green, M. A.; Hishikawa, Y.; Warta, W.; Dunlop, E. D.; Levi, D. H.; Hohl-Ebinger, J.; Ho-Baillie, A. W. H.

Solar Cell Efficiency Tables (version 50). *Prog. Photovoltaics* **2017**, *25*, 668-676.

27. Bisquert, J. Consolidation and Expansion of Perovskite Solar Cell Research. *J. Phys. Chem. Lett.* **2016**, *7*, 775-775.

28. Bisquert, J.; Qi, Y.; Ma, T.; Yan, Y. Advances and Obstacles on Perovskite Solar Cell Research from Material Properties to Photovoltaic Function. *ACS Energy Lett.* **2017**, *2*, 520-523.

29. Lopez-Varo, P.; Jiménez-Tejada, J. A.; García-Rosell, M.; Anta, J. A.; Ravishankar, S.; Bou, A. n.; Bisquert, J. Effects of Ion Distributions on Charge Collection in Perovskite Solar Cells. *ACS Energy Lett.* **2017**, *2*, 1450-1453.

30. Liu, F.; Zhang, Y.; Ding, C.; Kobayashi, S.; Izuishi, T.; Nakazawa, N.; Toyoda, T.; Ohta, T.; Hayase, S.; Minemoto, T.; Yoshino, K.; Dai, S.; Shen, Q. Highly Luminescent Phase-Stable CsPbI3 Perovskite Quantum Dots Achieving Near 100% Absolute Photoluminescence Quantum Yield. *ACS Nano* **2017**, *11*, 10373-10383.

31. Jellicoe, T. C.; Richter, J. M.; Glass, H. F. J.; Tabachnyk, M.; Brady, R.; Dutton, S. E.; Rao, A.; Friend, R. H.; Credgington, D.; Greenham, N. C.; Böhm, M. L. Synthesis and Optical Properties of Lead-Free Cesium Tin Halide Perovskite Nanocrystals. *J. Am. Chem. Soc.* **2016**, *138*, 2941-2944.

32. Pan, A.; He, B.; Fan, X.; Liu, Z.; Urban, J. J.; Alivisatos, A. P.; He, L.; Liu, Y. Insight into the Ligand-Mediated Synthesis of Colloidal CsPbBr3 Perovskite Nanocrystals: The Role of Organic Acid, Base, and Cesium Precursors. *ACS Nano* **2016**, *10*, 7943-7954.

33. Swarnkar, A.; Chulliyil, R.; Ravi, V. K.; Irfanullah, M.; Chowdhury, A.; Nag, A. Colloidal CsPbBr3 Perovskite Nanocrystals: Luminescence Beyond Traditional Quantum Dots. *Angew. Chem.* **2015**, *127*, 15644-15648.

34. Zhang, F.; Zhong, H.; Chen, C.; Wu, X.-g.; Hu, X.; Huang, H.; Han, J.; Zou, B.; Dong, Y. Brightly Luminescent and Color-Tunable Colloidal CH3NH3PbX3 (X= Br, I, Cl) Quantum Dots: Potential Alternatives for Display Technology. *ACS Nano* **2015**, *9*, 4533-4542.

35. Sun, S.; Yuan, D.; Xu, Y.; Wang, A.; Deng, Z. Ligand-Mediated Synthesis of Shape-Controlled Cesium Lead Halide Perovskite Nanocrystals via Reprecipitation Process at Room Temperature. *ACS Nano* **2016**, *10*, 3648-3657.

36. Protesescu, L.; Yakunin, S.; Bodnarchuk, M. I.; Krieg, F.; Caputo, R.; Hendon, C. H.; Yang, R. X.; Walsh, A.; Kovalenko, M. V. Nanocrystals of Cesium Lead Halide Perovskites (CsPbX3, X= Cl, Br, and I): Novel Optoelectronic Materials Showing Bright Emission with Wide Color Gamut. *Nano Lett.* **2015**, *15*, 3692-3696.

37. Swarnkar, A.; Marshall, A. R.; Sanehira, E. M.; Chernomordik, B. D.; Moore, D. T.; Christians, J. A.; Chakrabarti, T.; Luther, J. M. Quantum Dot-Induced Phase Stabilization of α-CsPbI3 Perovskite for High-Efficiency Photovoltaics. *Science* **2016**, *354*, 92-95.

38. Xing, G.; Mathews, N.; Lim, S. S.; Yantara, N.; Liu, X.; Sabba, D.; Grätzel, M.; Mhaisalkar, S.; Sum, T. C. Low-Temperature Solution-Processed Wavelength-Tunable Perovskites for Lasing. *Nat. Mater.* **2014**, *13*, 476-480.

39. Sutherland, B. R.; Hoogland, S.; Adachi, M. M.; Wong, C. T.; Sargent, E. H. Conformal Organohalide Perovskites Enable Lasing on Spherical Resonators. *ACS Nano* **2014**, *8*, 10947-10952.

40. Yakunin, S.; Protesescu, L.; Krieg, F.; Bodnarchuk, M. I.; Nedelcu, G.; Humer, M.; De Luca, G.; Fiebig, M.; Heiss, W.; Kovalenko, M. V. Low-Threshold Amplified Spontaneous Emission and Lasing from Colloidal Nanocrystals of Caesium Lead Halide Perovskites. *Nat. Commun.* **2015**, *6*, 8056.

41. Hoffman, J. B.; Zaiats, G.; Wappes, I.; Kamat, P. V. CsPbBr3 Solar Cells: Controlled Film Growth through Layer-by-Layer Quantum Dot Deposition. *Chem. Mater.* **2017**, *29*, 9767-9774.

42. Chen, J.; Chábera, P.; Pascher, T.; Messing, M. E.; Schaller, R.; Canton, S.; Zheng, K.; Pullerits, T. Enhanced Size Selection in Two-Photon Excitation for CsPbBr3 Perovskite Nanocrystals. *J. Phys. Chem. Lett.* **2017**, *8*, 5119-5124.

43. Palazon, F.; Almeida, G.; Akkerman, Q. A.; De Trizio, L.; Dang, Z.; Prato, M.; Manna, L. Changing the Dimensionality of Cesium Lead Bromide Nanocrystals by Reversible Postsynthesis Transformations with Amines. *Chem. Mater.* **2017**, *29*, 4167-4171.

44. Eperon, G. E.; Paterno, G. M.; Sutton, R. J.; Zampetti, A.; Haghighirad, A. A.; Cacialli, F.; Snaith, H. J. Inorganic Caesium Lead Iodide Perovskite Solar Cells. *J. Mater. Chem. A* **2015**, *3*, 19688-19695.

45. Tvrdy, K.; Frantsuzov, P. A.; Kamat, P. V. Photoinduced Electron Transfer from Semiconductor Quantum Dots to Metal Oxide Nanoparticles. *Proc. Natl. Acad. Sci. U.S.A.* **2011**, *108*, 29-34.

46. Maity, P.; Maiti, S.; Debnath, T.; Dana, J.; Guin, S. K.; Ghosh, H. N. Intraband Electron Cooling Mediated Unprecedented Photocurrent Conversion Efficiency of CdSxSe1-x Alloy QDs: Direct Correlation between Electron Cooling and Efficiency. *J. Phys. Chem. C* **2016**, *120*, 21309-21316.

47. Dana, J.; Anand, P.; Maiti, S.; Azlan, F.; Jadhav, Y.; Haram, S. K.; Ghosh, H. N. Inhibiting Interfacial Charge Recombination for Boosting Power Conversion Efficiency in CdSe{Au} Nanohybrid Sensitized Solar Cell. *J. Phys. Chem. C* **2017**, DOI: 10.1021/acs.jpcc.7b08448.

48. Ghosh, H. N.; Maiti, S.; Dana, J.; Tripathi, V. S. Direct Correlation of Excitonics with Efficiency in Core Shell Quantum Dot Solar Cell. *Chem. - Eur. J.*, DOI: 10.1002/chem.201705127.

49. Robel, I.; Kuno, M.; Kamat, P. V. Size-Dependent Electron Injection from Excited CdSe Quantum Dots into TiO2 Nanoparticles. *J. Am. Chem. Soc.* **2007**, *129*, 4136-4137.

50. Zidek, K.; Zheng, K.; Ponseca Jr, C. S.; Messing, M. E.; Wallenberg, L. R.; Chábera, P.; Abdellah, M.; Sundström, V.; Pullerits, T. Electron Transfer in Quantum-Dot-Sensitized ZnO Nanowires: Ultrafast Time-Resolved Absorption and Terahertz Study. *J. Am. Chem. Soc.* **2012**, *134*, 12110-12117.

51. Blackburn, J. L.; Selmarten, D. C.; Nozik, A. J. Electron Transfer Dynamics in Quantum Dot/Titanium Dioxide Composites Formed by in situ Chemical Bath Deposition. *J. Phys. Chem. B* **2003**, *107*, 14154-14157.

52. Hyun, B.-R.; Zhong, Y.-W.; Bartnik, A. C.; Sun, L.; Abruña, H. D.; Wise, F. W.; Goodreau, J. D.; Matthews, J. R.; Leslie, T. M.; Borrelli, N. F. Electron Injection from Colloidal PbS Quantum Dots into Titanium Dioxide Nanoparticles. *ACS Nano* **2008**, *2*, 2206-2212.

53. Jin, S.; Lian, T. Electron Transfer Dynamics from Single CdSe/ZnS Quantum Dots to TiO2 Nanoparticles. *Nano Lett.* **2009**, *9*, 2448-2454.

54. Wu, K.; Liang, G.; Shang, Q.; Ren, Y.; Kong, D.; Lian, T. Ultrafast Interfacial Electron and Hole Transfer from CsPbBr3 Perovskite Quantum Dots. *J. Am. Chem. Soc.* **2015**, *137*, 12792-12795.

55. Ishioka, K.; Barker, B. G.; Yanagida, M.; Shirai, Y.; Miyano, K. Direct Observation of Ultrafast Hole Injection from Lead Halide Perovskite by Differential Transient Transmission Spectroscopy. *J. Phys. Chem. Lett.* **2017**, *8*, 3902-3907.

56. Guijarro, N.; Lana-Villarreal, T.; Mora-Seró, I.; Bisquert, J.; Gómez, R. CdSe Quantum Dot-Sensitized TiO2 Electrodes: Effect of Quantum Dot Coverage and Mode of Attachment. *J. Phys. Chem. C* **2009**, *113*, 4208-4214.

57. Takagahara, T.; Takeda, K. Theory of the Quantum Confinement Effect on Excitons in Quantum Dots of

Indirect-Gap Materials. *Phys. Rev. B* **1992**, *46*, 15578.

58. Franceschetti, A.; Zunger, A. Pseudopotential Calculations of Electron and Hole Addition Spectra of InAs, InP, and Si Quantum Dots. *Phys. Rev. B* **2000**, *62*, 2614.

59. Leatherdale, C.; Bawendi, M. Observation of Solvatochromism in CdSe Colloidal Quantum Dots. *Phys. Rev. B* **2001**, *63*, 165315.

60. Liptay, W. Electrochromism and Solvatochromism. *Angew. Chem., Int. Ed.* **1969**, *8*, 177-188.

61. Shen, Q.; Ogomi, Y.; Chang, J.; Tsukamoto, S.; Kukihara, K.; Oshima, T.; Osada, N.; Yoshino, K.; Katayama, K.; Toyoda, T. Charge Transfer and Recombination at the Metal Oxide/CH3NH3PbClI2/Spiro-OMeTAD Interfaces: Uncovering the Detailed Mechanism Behind High Efficiency Solar Cells. *Phys. Chem. Chem. Phys.* **2014**, *16*, 19984-19992.

62. Klimov, V. I.; Mikhailovsky, A. A.; McBranch, D.; Leatherdale, C. A.; Bawendi, M. G. Quantization of Multiparticle Auger Rates in Semiconductor Quantum Dots. *Science* **2000**, *287*, 1011-1013.

63. Makarov, N. S.; Guo, S.; Isaienko, O.; Liu, W.; Robel, I.; Klimov, V. I. Spectral and Dynamical Properties of Single Excitons, Biexcitons, and Trions in Cesium-Lead-Halide Perovskite Quantum Dots. *Nano Lett.* **2016**, *16*, 2349-2362.

64. Park, Y.-S.; Guo, S.; Makarov, N. S.; Klimov, V. I. Room Temperature Single-Photon Emission from Individual Perovskite Quantum Dots. *ACS Nano* **2015**, *9*, 10386-10393.

65. Liu, Q.; Wang, Y.; Sui, N.; Wang, Y.; Chi, X.; Wang, Q.; Chen, Y.; Ji, W.; Zou, L.; Zhang, H. Exciton Relaxation Dynamics in Photo-Excited CsPbI3 Perovskite Nanocrystals. *Sci. Rep.* **2016**, *6*, 29442.

66. Zhang, Y. H.; Ding, C.; Wu, G. H.; Nakazawa, N.; Chang, J.; Ogomi, Y.; Toyoda, T.; Hayase, S.; KatayamA, K.; Shen, Q. Air Stable PbSe Colloidal Quantum Dot Heterojunction Solar Cells: Ligand-Dependent Exciton Dissociation, Recombination, Photovoltaic Property, and Stability. *J. Phys. Chem. C* **2016**, *120*, 28509-28518.

67. Shen, Q.; Ogomi, Y.; Das, S. K.; Pandey, S. S.; Yoshino, K.; Katayama, K.; Momose, H.; Toyoda, T.; Hayase, S. Huge Suppression of Charge Recombination in P3HT-ZnO Organic-Inorganic Hybrid Solar Cells by Locating Dyes at the ZnO/P3HT Interfaces. *Phys. Chem. Chem. Phys.* **2013**, *15*, 14370-14376.

68. Mondal, N.; Samanta, A. Complete Ultrafast Charge Carrier Dynamics in Photo-Excited All-Inorganic Perovskite Nanocrystals (CsPbX3). *Nanoscale* **2017**, *9*, 1878-1885.

69. Stockwell, D.; Yang, Y.; Huang, J.; Anfuso, C.; Huang, Z.; Lian, T. Comparison of Electron-Transfer Dynamics from Coumarin 343 to TiO2, SnO2, and ZnO Nanocrystalline Thin Films: Role of Interface-Bound Charge-Separated Pairs. *J. Phys. Chem. C* **2010**, *114*, 6560-6566.

70. Huang, J.; Huang, Z.; Jin, S.; Lian, T. Exciton Dissociation in CdSe Quantum Dots by Hole Transfer to Phenothiazine. *J. Phys. Chem. C* **2008**, *112*, 19734-19738.

71. Asbury, J. B.; Hao, E.; Wang, Y.; Ghosh, H. N.; Lian, T. Ultrafast Electron Transfer Dynamics from Molecular Adsorbates to Semiconductor Nanocrystalline Thin Films. *J. Phys. Chem. B* **2001**, *105*, 4545-4557.

72. Yoshihara, T.; Katoh, R.; Furube, A.; Murai, M.; Tamaki, Y.; Hara, K.; Murata, S.; Arakawa, H.; Tachiya, M. Quantitative Estimation of the Efficiency of Electron Injection from Excited Sensitizer Dye into Nanocrystalline ZnO Film. *J. Phys. Chem. B* **2004**, *108*, 2643-2647.

73. Hilgendorff, M.; Sundström, V. Dynamics of Electron Injection and Recombination of Dye-Sensitized TiO2 Particles. *J. Phys. Chem. B* **1998**, *102*, 10505-10514.

74.   Hannappel, T.; Burfeindt, B.; Storck, W.; Willig, F. Measurement of Ultrafast Photoinduced Electron Transfer from Chemically Anchored Ru-Dye Molecules into Empty Electronic States in a Colloidal Anatase TiO2 Film. *J. Phys. Chem. B* **1997**, *101*, 6799-6802.

75.   Marcus, R. A. On the Theory of Oxidation-Reduction Reactions Involving Electron Transfer. I. *J. Chem. Phys.* **1956**, *24*, 966-978.

76.   Sakata, T.; Hashimoto, K.; Hiramoto, M. New Aspects of Electron Transfer on Semiconductor Surface: Dye-Sensitization System. *J. Phys. Chem.* **1990**, *94*, 3040-3045.

77.   Murtaza, G.; Ahmad, I. First Principle Study of the Structural and Optoelectronic Properties of Cubic Perovskites CsPbM3 (M= Cl, Br, I). *Phys. B* **2011**, *406*, 3222-3229.

78.   Robertson, J. High Dielectric Constant Oxides. *Eur. Phys. J.: Appl. Phys.* **2004**, *28*, 265-291.

79.   Neukirch, A. J.; Nie, W.; Blancon, J.-C.; Appavoo, K.; Tsai, H.; Sfeir, M. Y.; Katan, C.; Pedesseau, L.; Even, J.; Crochet, J. J.; Gupta, G.; Mohite, A. D.; Tretiak, S. Polaron Stabilization by Cooperative Lattice Distortion and Cation Rotations in Hybrid Perovskite Materials. *Nano Lett.* **2016**, *16*, 3809-3816.

80.   Žídek, K.; Zheng, K.; Ponseca, C. S.; Messing, M. E.; Wallenberg, L. R.; Chábera, P.; Abdellah, M.; Sundström, V.; Pullerits, T. Electron Transfer in Quantum-Dot-Sensitized ZnO Nanowires: Ultrafast Time-Resolved Absorption and Terahertz Study. *J. Am. Chem. Soc.* **2012**, *134*, 12110-12117.

81.   Kojima, A.; Teshima, K.; Shirai, Y.; Miyasaka, T. Organometal Halide Perovskites as Visible-Light Sensitizers for Photovoltaic Cells. *J. Am. Chem. Soc.* **2009**, *131*, 6050-6051.